Characterization of tracer cascade in physical space

B.L. Hua, P. Klein, and G. Lapeyre

Laboratoire de Physique des Océans, IFREMER, BP 70; 29280 Plouzan; France
Also at Laboratoire de Météorologie Dynamique, 24 Rue Lhomond, 75230 Paris Cedex 05; France

Abstract. Geophysical turbulent fluids are characterized by the presence of organized energetic structures which control tracer transport and stirring, while enabling a tracer cascade down to the smallest scales. In order to understand the physical mechanisms involved in this turbulent tracer cascade, we focus on the dynamics underlying the formation of tracer gradients which are necessarily associated to this cascade. We show that the dynamics of tracer gradients in physical space is mainly governed by their orientation with respect to the compressional eigenvector of the strain tensor. This relative angle results from the competition between strain and the "effective rotation" (due to both vorticity and rotation of strain axes). The implication is that tracer gradients (be they passive or active) should align with specific directions of the flow field, which depends only on the local velocity and acceleration gradient tensors in physical space. Most of the tracer stirring is thus occurring at specific locations that can be identified analytically. These results have been confirmed by direct numerical simulations and enable a better characterization of the cascade in physical space.

1. Introduction

The widely observed tracer cascade toward small spatial scales in geophysical flows is known to result from stirring by mesoscale eddies. It corresponds to the formation of strong horizontal gradients, such as those indicated by the chlorophyl concentration at the sea surface as observed by satellite (Figure 1). Another observed characteristic is that horizontal gradients of different tracer fields are often found at the same locations in physical space. This is consistent with the interpretation that such locations result from the common topology of the underlying flow that advects the different tracer fields. This is observed for instance in Figure 2, which presents airborne measurements of different mixing ratios in the southern stratosphere, showing sharp horizontal gradients coinciding at several locations (*Tuck et al.*, 1992). On the other hand, the different strengths of the relative mixing ratios $|\nabla c|/c$ (where c is the mixing ratio) that are observed in Figure 2, are the result of the differences in the past history of the tracer fields, which may be caused by differences in their sources, forcings and sinks.
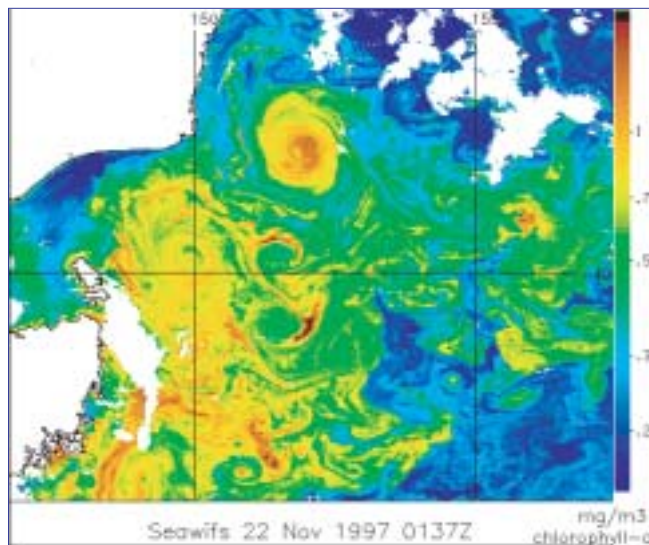

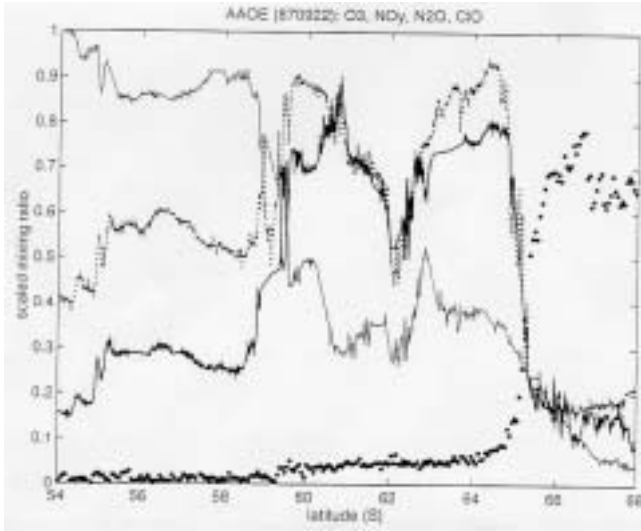**Figure 1.** Chlorophyll concentration as observed by SEA-WIFF

45

Figure 2. Different mixing ratios measured in the southern stratosphere (from *Tuck et al.*, (1992).
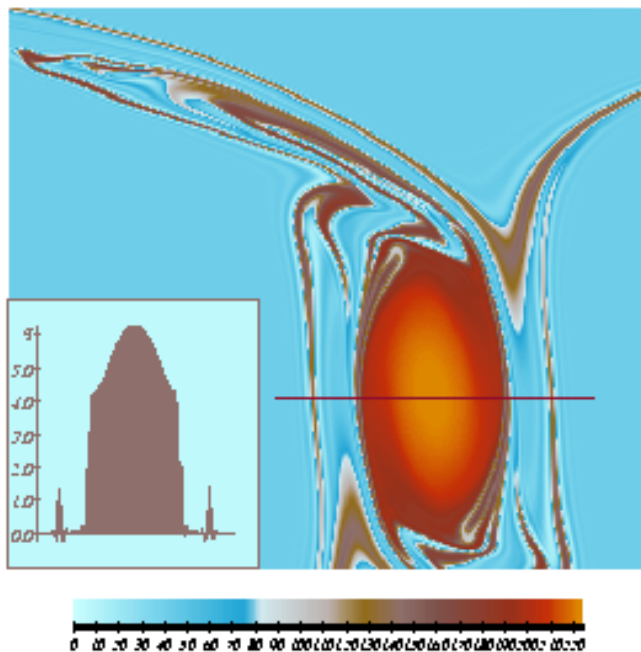

Figure 3. Vorticity field of an isolated vortex submitted to a externally prescribed strain field (*Mariotti et al.*, 1994).

However, the existence of intense gradients in tracer distribution does not always imply the occurrence of strong mixing of the tracer field. Figure 3 presents the vorticity distribution of an isolated vortex which is influenced by an externally prescribed strain field (*Mariotti et al.*, 1994). This setup leads to a constant erosion of the vortex structure, which is taking place through the ejection of filaments which will eventually be destroyed by small-scale mixing. However, as seen in the insert of Figure 3, the distribution of vorticity observed along a horizontal mid-section across the vortex shows a significant reinforcement with time of the gradients at the vortex boundary. Such a phenomenon is the opposite of mixing and corresponds to the formation of a barrier to transport that inhibits exchanges across the vortex boundary.
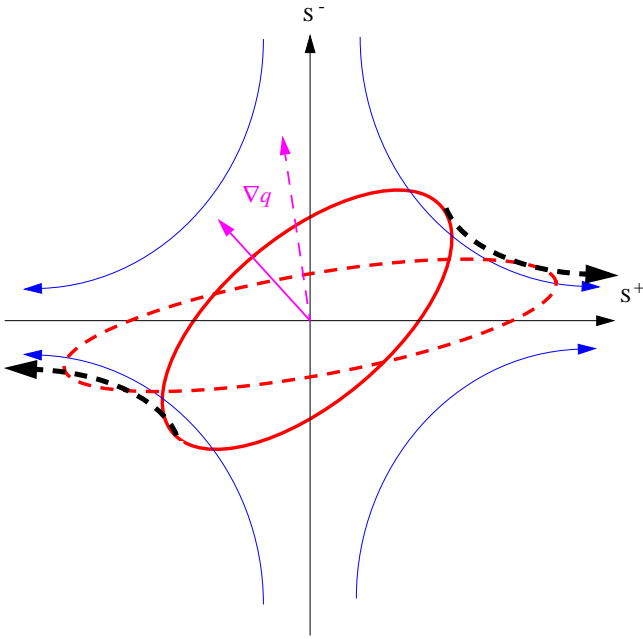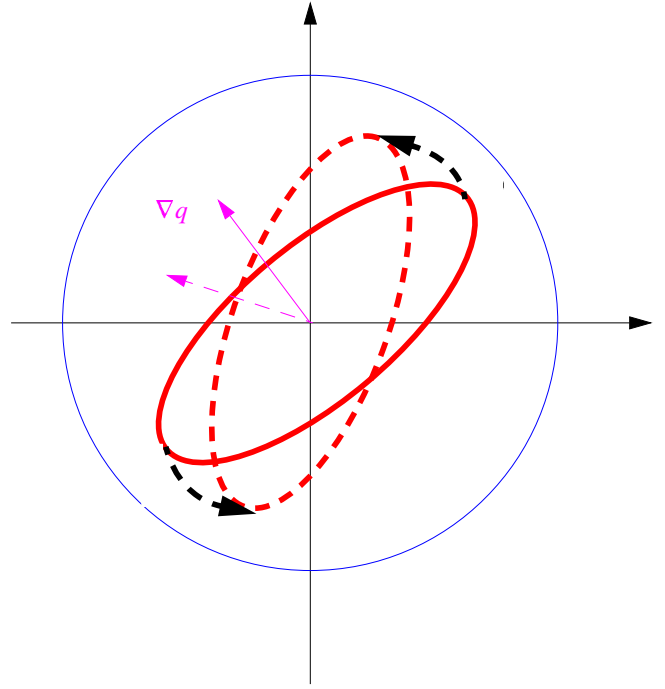
Our main purpose has been to attempt to characterize dynamically this tracer cascade in physical space. The specific objectives are to study the equations governing the dynamics of tracer gradients in order to localize the barriers to mixing as well as the regions of filament production. The chosen approach is to use information from **both the velocity $\vec{u}$ and acceleration fields** $\frac{D\vec{u}}{Dt}$ in order to go beyond the simple kinematic approach of the chaotic advection literature, which relies on the sole knowledge of the velocity field.

In what follows, we have moreover made the assumption that as far as oceanic mesoscale eddies are concerned, the classical framework of the quasigeostrophic turbulence is a valid first step.

The paper is organized as follows. We first recall the basic ingredients that influence the evolution of tracer gradient by considering simple flows (section 2). The equations governing the dynamics of tracer gradients are then studied in section 3, leading to the prediction of preferred alignment of tracer gradients with specific orientations for different regions of the flow, which are found to depend on the tensors of velocity gradient and acceleration gradients $\nabla \vec{u}$ and $\nabla \frac{D\vec{u}}{Dt}$. Section 4 presents results from numerical simulations of two-dimensional turbulence in free-decay, providing evidence of statistical validation of alignment properties of the tracer cascade in physical space. Section 5 summarizes our results and mentions possible applications of the tracer gradient dynamics.

2. Simple flows

For a pure strain field, the streamfunction field $\psi = \sigma\, xy$ corresponds to the blue isolines of Figure 4, where σ denotes the strain-rate magnitude. An initial tracer blob (red continuous isoline) will be stretched with time into an elongated pattern (the red dotted isoline) and the tracer gradient ∇q (black vector) will tend to align

Figure 4. Pure strain field

Figure 5. Pure vorticity field

Figure 6. Finite size axisymmmetric vortex

with time with the compressional principal axis of the strain tensor (denoted by $\mathbf{S}^-$ in Figure 4). This alignment is associated with an exponential growth of the tracer gradient norm.

In the case of a pure vorticity field the streamfunction field is $\psi = \frac{\omega}{2}(x^2 + y^2)$, where ω denotes the vorticity. The initial tracer blob (red continuous isoline) simply rotates with time (the red dotted isoline) and so does the tracer gradient vector (Figure 5). There is no growth of the tracer gradient norm. The above simple limits can be obtained from the results of *Okubo* (1970) and *Weiss* (1991). For a passive tracer q that obeys the conservation equation
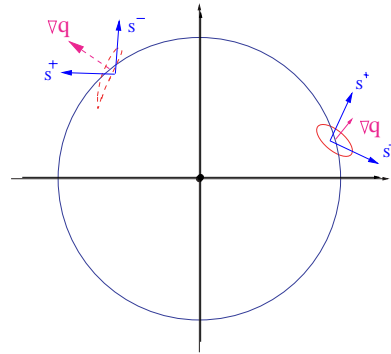
$$\frac{Dq}{Dt} = 0,$$

its gradient will obey

$$\frac{D\nabla q}{Dt} = -[\nabla \vec{u}]^* \ \nabla q. \tag{1}$$

$[\nabla \vec{u}]^*$ denotes the transpose of the velocity gradient tensor for which eigenvalues are $\pm\lambda^{1/2}$, where $\lambda = \sigma^2 - \omega^2$ depends on the competition between strain and vorticity. Both authors made the assumption that $[\nabla \vec{u}]^*$ is slowly varying along a Lagrangian trajectory ($\frac{D\nabla \vec{u}}{Dt} \sim 0$) so that the tracer gradient equation can be integrated, yielding

$$\nabla q = \nabla q_0 \ \exp(\pm\lambda^{1/2} \ t).$$

Thus in regions where the strain rate dominates ($\lambda > 0$), there is an exponential growth of the gradient norm,

while in regions where vorticity dominates ($\lambda < 0$), the solution corresponds to a simple rotation of the gradient vector.

It is easy to find simple counterexamples where the Okubo-Weiss results do not hold (*Pierrehumbert and Yang*, 1993). Consider the case of an axisymmetric vortex of finite size, such that outside the vortex core, the vorticity is $\omega = 0$, while the strain rate is $\sigma \neq 0$ and streamlines are still circular. In such a region, $\lambda = \sigma^2 - \omega^2 = \sigma^2 > 0$ and the Okubo-Weiss criterion predicts an exponential growth. However, such a case can be integrated analytically (*Lapeyre et al.*, 1999) and the solution is found to correspond to a continuous rotation of the tracer gradient with a linear growth of

its norm with time. The Okubo-Weiss criterion fails because the rotation of the principal axes of the strain-rate tensor has not been taken into account, and this implies $\frac{D\nabla \vec{u}}{Dt} \neq 0$. Along the circular Lagrangian trajectories (Figure 6), the principal axes constantly rotate so that the tracer gradient vector cannot align with the compressional strain axis, and the initial tracer blob (continuous red line) is mostly linearly distorted with time. Other simple counterexamples can be constructed, involving a rotation of the strain-rate principal axes, where the Okubo-Weiss criterion fails and can be found for instance in *Young* (1999).

3. Dynamics of tracer gradient

The equation that governs the dynamics of tracer gradient (1) can be explicit as

$$\frac{D\nabla q}{Dt} = -\frac{1}{2}\begin{pmatrix} \sigma_n & \sigma_s + \omega \\ \sigma_s - \omega & -\sigma_n \end{pmatrix}\nabla q, \qquad (2)$$

where the following quantities have been used

$$\begin{array}{rcl} \sigma_n & = & \partial_x u - \partial_y v \\ \sigma_s & = & \partial_x v + \partial_y u \\ \sigma^2 & = & \sigma_n^2 + \sigma_s^2 \\ \omega & = & \partial_x v - \partial_y u. \end{array}$$

It is important to note that equation (2) is a vector equation and corresponds to two degrees of freedom that can be chosen as the tracer gradient norm $|\nabla q|$ and its orientation θ,

$$\nabla q = |\nabla q|\begin{pmatrix} \cos\theta \\ \sin\theta \end{pmatrix}.$$

An angle ϕ that characterizes the orientation of the strain axes with respect to the coordinate axis (Figure 7) can be introduced

$$\begin{pmatrix} \sigma_n \\ \sigma_s \end{pmatrix} = \sigma\begin{pmatrix} \sin 2\phi \\ \cos 2\phi \end{pmatrix}.$$

The two scalar equations for the norm $|\nabla q|$ and the gradient orientation θ are derived in *Lapeyre et al.* (1999).

$$\frac{D\log|\nabla q|^2}{Dt} = -\sigma\sin(2(\theta + \phi))$$

$$2\frac{D\theta}{Dt} = \omega - \sigma\cos(2(\theta + \phi))$$

Both scalar equations depend only on the relative angle

$$\zeta = 2(\theta + \phi)$$

(Figure 7) between ∇q and the compressional axis $\mathbf{S}^-$. We have seen in previous simple examples that it is this relative angle that determines the growth rate with
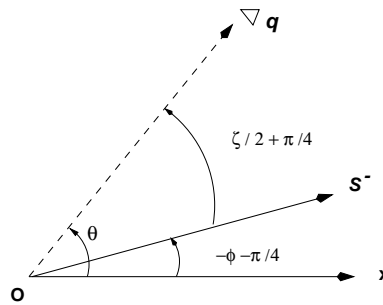

Figure 7. definition of angles ϕ, θ and ζ

time of the gradient norm. Introducing a nondimensional Lagrangian time which is related to the strain-rate magnitude

$$\tau = \int_0^t \sigma(t')dt',$$

one can rewrite both scalar equations as

$$\frac{D\log|\nabla q|^2}{D\tau} = -\sin\zeta$$

$$\frac{D\zeta}{D\tau} = r - \cos\zeta. \qquad (3)$$

The orientation equation (3b) involves a nondimensional parameter r which is defined as

$$r = \frac{\omega + 2D\phi/Dt}{\sigma} = \frac{effective\ rotation}{strain\ rate}$$

The dimensionless parameter r is the ratio between "effective rotation"[1] in the strain basis (i.e. the rotation effects due to both the vorticity and the rotation of the principal axes of the strain-rate tensor) and the magnitude of the strain rate (which tends to align the gradient with a strain eigenvector).

An important remark is that r remains invariant in a change of coordinates involving solid body rotation, while the Okubo-Weiss eigenvalues λ do not remain invariant in such a change of coordinates. The new physics that have been taken into account correspond to the quantity $\frac{D\phi}{Dt}$ that takes into account the fact that the principal axes of strain can vary along a Lagrangian trajectory, also implying that $\frac{D\nabla\vec{u}}{Dt} \neq 0$.

Note that the dynamics of the orientation equation (3b) is completely independent of the actual value of the gradient norm $|\nabla q|$, and the solution to (3b) will depend on the actual value of r, whether $r > 1$ or $r < 1$.

Strain-dominated regions

By definition, this corresponds to $|r| < 1$. Making the weaker assumption that both r and the strain mag-

---

[1]We follow the terminology of *Dresselhaus and Tabor* (1991).

nitude σ are slowly varying along a Lagrangian trajectory, the equation for the orientation ζ has two fixed points $\zeta_{\pm} = \pm\arccos r$, an unstable one ζ_+, and a stable one ζ_-. One expects a rapid alignment of the tracer gradient with the stable orientation ζ_-, leading to an exponential growth rate of $\sigma\sqrt{1-r^2}$ for the tracer gradient norm (*Lapeyre et al.*, 1999). Conversely, the unstable orientation ζ_+ corresponds to a strong decay of $|\nabla q|$. In the case where $|r| = 1$, there is an algebraic growth of $|\nabla q|^2$ with time.

"Effective rotation"-dominated regions

In regions where the effective rotation dominates, $|r| > 1$. There is no fixed point solution to equation (3) and one has a nonuniform rotation of gradient. Since $\frac{D\zeta}{Dt}$ is variable the gradient tends to spend most of its time near the direction with minimal rotation rate ($D^2\zeta/Dt^2 = 0$). The most probable orientation of this direction is α such that (*Klein et al.*, 2000)

$$\alpha = \arctan\left(\frac{s}{r}\right) + (1 - sign(r))\frac{\pi}{2},$$

which depends on another nondimensional parameter s which is defined as

$$s = -\frac{D(\sigma^{-1})}{Dt},$$

which measures how rapidly the stirring time scale σ^{-1} varies along a Lagrangian trajectory. In such a situation, the gradient norm presents only a weak growth or decay rate of $-\sigma\, s/\sqrt{r^2 + s^2}$.

The two nondimensional parameters r and s suffice to characterize the topology of stirring as well as the time evolution of the tracer gradient magnitude (growth or decay). For instance, a saddle point corresponds to the values $r = 0$ and $s = 0$, the axisymmetric vortex flow to the values $|r| = 1$ and $s = 0$ and the strong rotation limit to $|r| \gg 1$.

Finally, one can show that r and s depend on both the velocity gradient tensor $\nabla\vec{u}$ and on the acceleration gradient tensor $\nabla\frac{D\vec{u}}{Dt}$.

4. Numerical simulations

In order to test the above analytical predictions for alignment of the tracer gradient, numerical simulations of freely decaying turbulence have been performed at a resolution of $(1024)^2$.

Figure 8 displays the vorticity field in a portion of the domain where a strong vorticity filament is being stretched between two cyclonic vortices. The color code is such that red/brown corresponds to positive vorticity and blue to negative values. The corresponding field
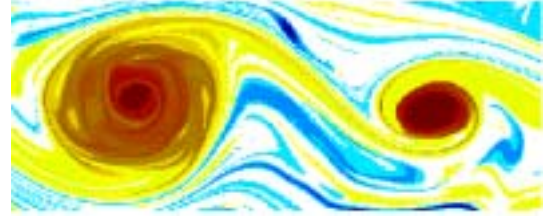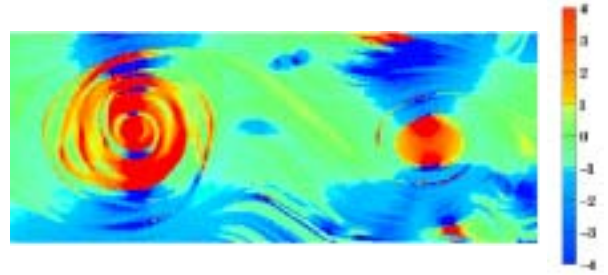

Figure 8. vortictiy ω

Figure 9. $r = \frac{\omega + 2D\phi/Dt}{\sigma}$

of the parametere r is given in Figure 9, where green indicates regions where the strain dominates, blue and red correspond to regions where effective rotation dominates. In the latter regions, red corresponds to the case when vorticity contributes the largest part of the effective rotation while blue corresponds to the opposite situation. Strips of yellow correspond to $|r| = 1$.

The parameter r presents sharp transitions and also a smooth behaviour along the longitudinal direction of the filamentary patterns. The vortex cores are regions with $r < -1$ because of large ω. Their periphery is composed of regions with $r^2 < 1$ because of large σ and regions with $r > 1$ because of large $\frac{D\phi}{Dt}$. For each vortex, we observe opposite signs of r between its core and the part on its periphery where effective rotation is strong. In these regions, $\omega + 2\frac{D\phi}{Dt}$ is dominated by $2\frac{D\phi}{Dt}$ which is of opposite sign of ω. This indicates that a characterization of the stirring properties of vortices must take into account this rotation rate.

The results for the alignment of the tracer gradient in strain-dominated regions, where $r < 1$, are checked against the analytical prediction $\zeta \approx \zeta_-$ in Figure 10, which presents the joint p.d.f. of $\zeta + \pi/2$ and r, and the bold curve is $\cos\zeta$. The relation $\cos\zeta \sim r$ is well corroborated and this strongly validates the analytical solution. On the other hand, a joint p.d.f. between $\zeta + \pi/2$ and ω/σ, which corresponds to the assumption of Okubo-Weiss that implies $\frac{D\phi}{Dt} = 0$, does not present such a correlation, and no alignment occurs for Okubo-Weiss criterion (Figure 11). This further emphasizes the quantitative importance of the rotation of the strain
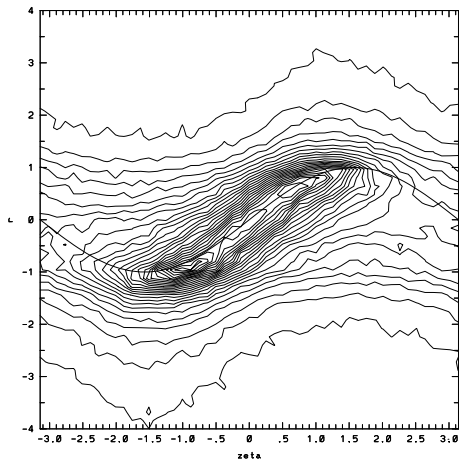
Figure 10. PDF of $\zeta + \pi/2$ and $r = \frac{\omega + 2\frac{D\phi}{Dt}}{\sigma}$
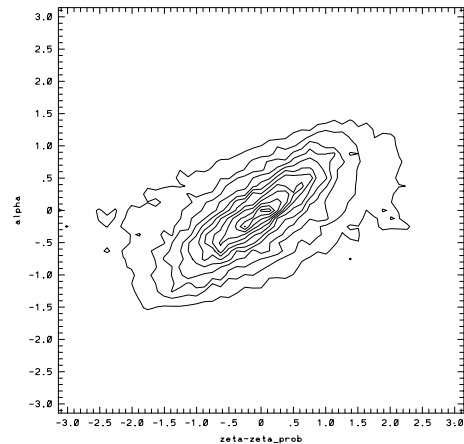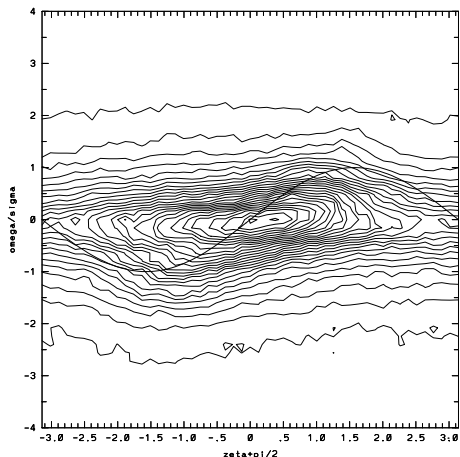

Figure 12. PDF of ζ and α

the parameter r

$$r = \frac{\omega + 2\frac{D\phi}{Dt}}{\sigma},$$

that measures the competition between the strain rate and the effective rotation which takes into account both the vorticity and the rotation rate of the principal axes of the strain-rate tensor along a Lagrangian trajectory (*Lapeyre et al.*, 1999). Strong gradient growth occurs when $|r| < 1$. The second regime needs another parameter s

$$s = -\frac{D(\sigma^{-1})}{Dt}$$

that measures the variation of the stirring time scale (σ^{-1}) along a Lagrangian trajectory (*Klein et al.*, 2000), and weaker growth/decay of the tracer gradient occurs for $|r| > 1$.

In both regimes, the flow topology enforces preferred orientations for the tracer gradient vector, which will depend on both **local properties of the velocity** gradient tensor $\nabla \vec{u}$ and also on the **long-range spatial influence of the acceleration** gradient tensor $\nabla \frac{D\vec{u}}{Dt}$ (*Ohkitani and Kishiba*, 1995; *Hua and Klein*, 1998). Both $\nabla \vec{u}$ and $\nabla \frac{D\vec{u}}{Dt}$ are entirely diagnostic for quasi-geostrophic dynamics and their computation only involves the resolution of Poisson problems in which right-hand sides are nonlinear functions of the streamfunction field at a given time (*Hua et al.*, 1998).

These predictions based on tracer gradient dynamics have been applied to two other problems which are also related to the more general issue of stirring.

The first case corresponds to the detection of invariant manifolds (i.e. the attracting/repelling material lines associated with local maxima of particle dispersion or equivalently to local maxima of tracer gradients) by

Figure 11. PDF of $\zeta + \pi/2$ and ω/σ for Okubo-Weiss results

axes.

The results for the alignment of the tracer gradient for regions where effective rotation dominates, $r > 1$ are checked against the analytical prediction $\zeta \approx \alpha$ in Figure 12, where the joint p.d.f. of ζ and α is plotted. Again, the numerical simulations confirm that there exist preferred directions of alignment of the tracer gradient that depends on r and s.

5. Discussion

To summarize, the dynamics of tracer gradients as a function of the flow topology can be captured by two regimes. The first one is well characterized solely by

computing the persistence of hyperbolicity defined as

$$\tau_r = \int_{|r|<1} \sigma dt,$$

along a Lagrangian trajectory in regions where $|r| < 1$ for a finite time. This technique enables us to locate the presence of such manifolds in the immediate vicinity of coherent vortices, as well as in the "far field" (*Lapeyre et al.*, 2001). For the second case, we have applied the analytical prediction of the time evolution of the tracer gradient norm to the predictability problem with the aim of identifying the regions of most rapid growth of the dynamical structures (*Riviére et al.*, 2001). The underlying idea is that initial perturbations that are responsible for the rapid growth of the structures in a given flow can be viewed as perturbations of the initial potential vorticity field of the flow. As such, their dynamics are closely linked in physical space to the regions which present the largest growth in potential vorticity gradients. Potential vorticity being a tracer field, the above analytical predictions can be used to identify the "sensitive" regions of most rapid growth.

References

Dresselhaus, E., and M. Tabor, The stretching and alignment of material elements in general flow fields, *J. Fluid Mech., 236*, 415–444, 1991.

Hua, B. L., and P. Klein, An exact criterion for the stirring properties of nearly two-dimensional turbulence, *Physica D, 113*, 98–110, 1998.

Hua, B. L., J. C. McWilliams, and P. Klein, Lagrangian accelerations in geostrophic turbulence, *J. Fluid Mech., 366*, 87–108, 1998.

Klein, P., B. L. Hua, and G. Lapeyre, Alignment of tracer gradients in two-dimensional turbulence using second order Lagrangian dynamics, *Physica D, 146*, 246–260, 2000.

Lapeyre, G., P. Klein, and B. L. Hua, Does the tracer gradient vector align with the strain eigenvectors in 2-D turbulence ?, *Phys. Fluids A, 11*, 3729-3737, 1999.

Lapeyre, G., B. L. Hua, and B. Legras, Comments on "Finding invariant manifolds in two-dimensional velocity fields", *Chaos*, in press.

Mariotti, A., B. Legras, and D. G. Dritschel, Vortex stripping and the erosion of coherent structures in two-dimensional flows, *Phys. Fluids A, 6*, 3954–3962, 1994.

Ohkitani, K., and S. Kishiba, Nonlocal nature of vortex stretching in an inviscid fluid, *Phys. Fluids A, 7*, 411–421, 1995.

Okubo, A., Horizontal dispersion of floatable particles in the vicinity of velocity singularity such as convergences, *Deep-Sea Res., 17*, 445–454, 1970.

R. T. Pierrehumbert, and H. Yang, Global chaotic mixing on isentropic surfaces, *J. Atmos. Sci., 50*, 2462–2480, 1993.

Riviére, G.,B. L. Hua and P. Klein, An analytical Lagrangian approach to predictability based on potential vorticity gradients, *what?*, , 2001 in prep.

Tuck, A. F., T. Davies, S. J. Hovde, M. Noguer-Alba, D. W. Fahey, S. R. Kawa, K. K. Kelly, D. M. Murphy, M. H. Profitt, J. J. Margitan, M. Loewenstein, J. R. Podolske, S. E. Strahan, and K. R. Chan, Polar stratospheric cloud processed air and potential vorticity in the northern hemisphere lower stratosphere at mid-latitudes during winter, *J. Geophys. Res., 97*, 7883–7904, 1992.

Weiss, J., The dynamics of enstrophy transfer in two-dimensional hydrodynamics, *Physica D, 48*, 273–294, 1991.

Young, W. R., Lecture notes on Stirring and Mixing, *Geophysical Fluid Dynamics Summer School* 1999, Woods Hole.